Polariton Spin Whirls

P. Cilibrizzi,[1] H. Sigurdsson,[2,3] T.C.H. Liew,[2] H. Ohadi,[1] S. Wilkinson,[1] A. Askitopoulos,[1] I. A. Shelykh,[2,3,4] and P. G. Lagoudakis[1]

[1]*School of Physics and Astronomy, University of Southampton, Southampton, SO17 1BJ, United Kingdom*
[2]*Division of Physics and Applied Physics, Nanyang Technological University 637371, Singapore*
[3]*Science Institute, University of Iceland, Dunhagi-3, IS-107 Reykjavik, Iceland*
[4]*ITMO University, St. Petersburg, 197101, Russia*

(Dated: September 14, 2015)

We report on the observation of spin whirls in a radially expanding polariton condensate formed under non-resonant optical excitation. Real space imaging of polarization- and time-resolved photoluminescence reveal a spiralling polarization pattern in the plane of the microcavity. Simulations of the spatiotemporal dynamics of a spinor condensate reveal the crucial role of polariton interactions with a spinor exciton reservoir. Harnessing spin dependent interactions between the exciton reservoir and polariton condensates allows for the manipulation of spin currents and the realization of dynamic collective spin effects in solid state systems.

I. INTRODUCTION

Phase transitions in atomic Bose Einstein condensates (BECs) are associated with symmetry breaking and the appearance of topological defects. In quantum fluids the appearance of quantized vortices in a rotating condensate marks the transition to the superfluid regime [1]. In the case of spinor condensates the extra degree of freedom provided by the spin, gives rise to complex spin patterns, known as merons [2] and skyrmions [3]. These structures appear as intricate spin textures due to the rotation of the spins across the condensate induced by dipole-dipole interactions [2]. Spontaneous rotation of the spin textures and breaking of chiral symmetry has been reported in a spinor BEC with ferromagnetic interactions [4]. Skyrmions and other nontrivial spin structures have also been observed in 2D superfluid Fermi gas[5], topological insulators[6] and magnetic thin film materials[7]. This tremendous interest in exploring the physics of spin textures is motivated by their strong relation with fundamental phenomena, such as the spin Hall effect in semiconductors[8,9] and spontaneous symmetry breaking in BECs[10], but also by their potential in future applications, such as low-power magnetic data storage[11] and logic devices[12].

In this work, a dynamical spin texture in polariton microcavity is studied for the first time. Polaritons are bosonic quasiparticles formed by the strong coupling between quantum well excitons and the photonic mode of a planar semiconductor microcavity [13,14]. When the polariton population is increased above a threshold density, stimulated scattering leads polaritons to macroscopically occupy the ground state of the dispersion and form a *nonequilibrium* BEC[15,16]. Being bosons, polaritons possess an integer spin with two possible projections of the angular momentum ($S_z = \pm 1$) on the structural growth axis (z) of the microcavity. Their spin can be optically accessed by means of polarization measurements and described theoretically within the pseudospin formalism[17]. One of the most important effects involving polariton spin, is the so called optical spin Hall effect (OSHE) [18], observed in both polaritonic [19] and photonic [20] microcavities. The effect is enabled by the energy splitting between transverse-electric (TE) and transverse-magnetic (TM) polarized modes [21], which occurs naturally in microcavities and results in spin currents propagating over hundreds of microns in both resonant [22] and non-resonant configurations [23]. Due to the OSHE, the long range coherence [24] and fast spin dynamics [25], polaritons have been proposed as a potential candidate for the realization of a new generation of spinoptronic devices [26]. In this regard, the contribution of a spin dependent exciton reservoir has not been considered thoroughly, although in non-resonant experiments and in the proximity of the excitation spot, exciton interactions dominate over other types of interactions[27] and can directly affect the spin dynamics of polaritons[28].

In this Letter, we report on the experimental observation of spin whirls in the radial expansion of a polariton condensate formed under non-resonant optical excitation in a GaAs quantum well (QW) microcavity. A spin whirl is a spin texture that rotates in the microcavity plane due to the interplay between the TE-TM splitting and the interaction with an exciton reservoir. The TE-TM splitting alone is responsible for the formation of symmetric 2D spin textures, which is intrinsically a linear effect [22]. As a consequence, the orientation of the spin current in the microcavity plane remains fixed in time. However, in the case of a radially expanding condensate, nonlinear interactions with the exciton reservoir at the spatial center of the condensate produce a spiralling effect, which culminates in a coherent rotation of the whole spin texture. The rotation is traced in an inherent spin imbalance in the exciton reservoir that acts as an effective magnetic field due to the anisotropic exciton-polariton interactions. We observe the spiralling effect in both time- and energy-resolved measurements. Simulations based on the Gross-Pitaevskii equation (GPE) coupled with an exciton reservoir unveil the role of the spin imbalanced exciton reservoir in reproducing the experimental obser-

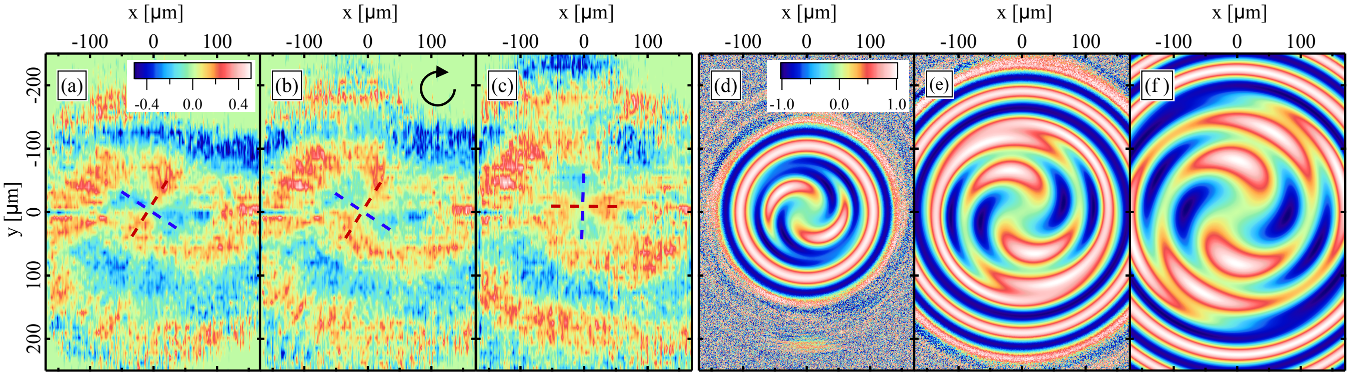

Figure 1. Snapshots of the spatio-temporal dynamics of the degree of circular polarization S_z under non-resonant linearly polarised excitation at: (a) 38 ps, (b) 41 ps and (c) 46 ps showing the clockwise rotation of the spin texture within the microcavity plane (zero time is defined at the PL onset, see the full dynamics in supplementary video S1). (d-f) Theoretical simulations showing the circular Stokes vector of the spin whirls at: (d) 30 ps, (e) 45 ps and (f) 60 ps. The parameters used in the simulations are reported in Ref. [34].

vations.

The paper is organized as follows: In Sec. II we describe the sample and the experimental setup. In Sec. III we report the main experimental and theoretical results showing the rotating spin textures in the plane of the microcavity, i.e. the spin whirls. In Sec. IV the theoretical model is presented and explained. In Sec. V we discuss the physical origin of the spin whirls and present additional measurements. Conclusions and perspectives are reported in Sec. VI.

II. SAMPLE AND EXPERIMENTAL SETUP

We use a $5\lambda/2$ AlGaAs/GaAs microcavity, with four sets of three QWs, characterized by a cavity photon lifetime of ~ 9 ps and a Rabi splitting of 9 meV. All the data presented here are recorded at negative exciton-photon detuning, $\Delta = -4$ meV, and under a non-resonant (1.653 eV) pulsed optical excitation (250 fs, 80 MHz) of 7 mW, focused to a ~ 2 μm FWHM spot using a 0.4 numerical aperture objective. The excitation beam is linearly polarised with polarization extinction ratio higher than 1:10^3. Photoluminescence (PL) is then collected in reflection geometry through the same objective, analyzed by a polarimeter composed of a $\lambda/2$ or $\lambda/4$ waveplate and a linear polarizer and projected on the entrance slit of a streak camera, with 2 ps temporal resolution (see section 1 (S1) of the supplementary information [29] for details).

III. ROTATING SPIN TEXTURE: THE SPIN WHIRLS

Under non-resonant linearly polarized excitation, time and polarization resolved measurements reveal a clockwise rotation of the entire spin texture in the plane of the microcavity at an angular velocity of about 0.11 rad/ps. This is shown in Figs. 1 (a-c) for the z-component of the Stokes vector, i.e., the degree of circular polarization, $S_z = (I_{\psi_+} - I_{\psi_-})/I_{tot}$, with I_{ψ_+} and I_{ψ_-} being the measured intensity of the two circular polarization components and $I_{tot} = I_{\psi_+} + I_{\psi_-}$ (see supplementary information [29], video S1 for full dynamics). The non-resonant excitation creates a reservoir of hot excitons, which rapidly relaxes to populate the lower polariton dispersion and form a polariton condensate [15]. At the pump spot position, due to the repulsive interactions between polaritons and the exciton reservoir, the condensate is blueshifted in energy. Outside the pump spot, this potential energy is converted to kinetic energy with an in-plane wavevector (here k $\leq 2.8\,\mu m^{-1}$) determined by the cavity lifetime and the gradient of the potential [16]. Thus, highly focused Gaussian excitation (~ 2 μm FWHM), produces a cylindrically symmetric potential that leads to the radial expansion of polaritons in the plane of the microcavity (see video S2).

IV. THEORETICAL MODEL

To accurately model the spin dynamics in the exciton-polariton system, an open-dissipative Gross-Pitaevskii equation (1) describes the polariton spinor order parameter ($\Psi_\pm$), which is then coupled with the exciton reservoir density ($\mathcal{N}_\pm$) [30]:

$$i\hbar\frac{d\Psi_\pm}{dt} = \Big[\hat{E} - \frac{i\hbar}{2\tau_p} + \alpha|\Psi_\pm|^2 + G\sigma_\pm P(\mathbf{r},t) + \Big(g_R + \frac{i\hbar r_c}{2}\Big)\mathcal{N}_\pm\Big]\Psi_\pm + \hat{H}_{\mathrm{LT}}\Psi_\mp, \qquad (1)$$

$$\frac{d\mathcal{N}_\pm}{dt} = -\left(\frac{1}{\tau_x} + r_c|\Psi_\pm|^2\right)\mathcal{N}_\pm + \sigma_\pm P(\mathbf{r},t). \qquad (2)$$

These equations model the process of polaritons being generated from a hot exciton reservoir and then scattered into the ground state of the condensate. The coupled equations take into account the energy blueshift of the condensate due to interactions with excitons (with interaction strength g_R). $\hat{E}$ is the condensate kinetic energy, τ_p and τ_x are the polariton and exciton lifetimes respectively. It has been shown that the dominant component of interactions between polaritons comes from the exchange interaction[31]. In our model, the same-spin polariton interactions strength is characterized by the parameter α. We neglect interactions between polaritons with opposite spins, which are typically smaller in magnitude [32] at energies far from the biexciton resonance [33]. The exciton reservoir is driven by a Gaussian pump, $P(\mathbf{r}, t)$, as in the experiment, and feeds the polariton condensate with a condensation rate (r_c). An additional pump-induced shift is described by the interaction constant G to take into account other excitonic contribution to the blueshift [30]. The polarization of the pump is controlled by the parameters σ_+ and σ_- (e.g., a horizontally polarized pump would correspond to $\sigma_+ = \sigma_- = 1$). $\hat{H}_{\mathrm{LT}}$ is the TE-TM splitting which mixes the spins of the polaritons:

$$\hat{H}_{\mathrm{LT}} = \frac{\Delta_{LT}}{k_{LT}^2}\left(i\frac{\partial}{\partial x} \pm \frac{\partial}{\partial y}\right)^2, \tag{3}$$

with Δ_{LT} being half TE-TM splitting at wavevector k_{LT}. The TE-TM splitting is defined by the ratio Δ_{LT}/k_{LT}^2, while the in-plane wavevector of polaritons is given by the operator in the round brackets. The parameters used in the simulations are reported in Ref.[34].

V. DISCUSSION

A. Different pump polarizations give rise to different spin textures

In Figure 2, the theoretical circular Stokes polarization patterns obtained with circularly [Fig. 2 (a)] and linearly [Fig. 2 (b)] polarized pump are shown. In the nonlinear regime, the circular pump allows for injection of a single spin condensate that due to OSHE evolves to concentric rings of alternating spin [23], as shown in Fig. 2 (a). The cylindrically symmetric patterns observed here are due to the fact that the polariton pseudospin, directed along the z-axis in the Poincaré sphere, is always perpendicular to the effective magnetic field, lying on the x-y plane. Under linearly polarized pump [Fig. 2 (b)] due to the absence of spin imbalance in the exciton reservoir, the fermionic component of excitons produces strong exchange coupling between bright and dark states that force the condensate to be linearly polarized[35]. In this case, the typical OSHE pattern is retrieved due to the Stokes vector precessing at 45° to the x, y axis [18]. It has been predicted that under linear excitation the condensate forms a Skyrmion pattern [36].

For the creation of polarisation symmetry breaking textures such as the spin whirls observed here, a spin imbalance is necessary. Although we excite with a highly linearly polarized beam (extinction ratio higher than $1:10^3$), an ellipticity is created due to the high numerical aperture of the focusing lens. Indeed, the electric field of a linearly polarized beam, when focused by a high-NA objective, acquires non-zero components in the two directions perpendicular to the polarization of the incident field (i.e., at the focal plane the electric field vector sweeps an ellipse) [37,38]. Thus, the tight focus of a linearly polarized excitation beam, breaks the rotational symmetry of the σ_+ and σ_- polarizations and introduces an ellipticity in the pump spot. We have measured an ellipticity of 10% for the excitation conditions used in the experiment (see supplementary information [29], S3).
In the simulations, we introduce a 10% ellipticity in the linearly polarized pump, i.e., elliptical pulse with (σ_+, σ_-)=(1, 0.9), and observe that the circular polarization patterns rotate, as shown in Fig. 2 (c).

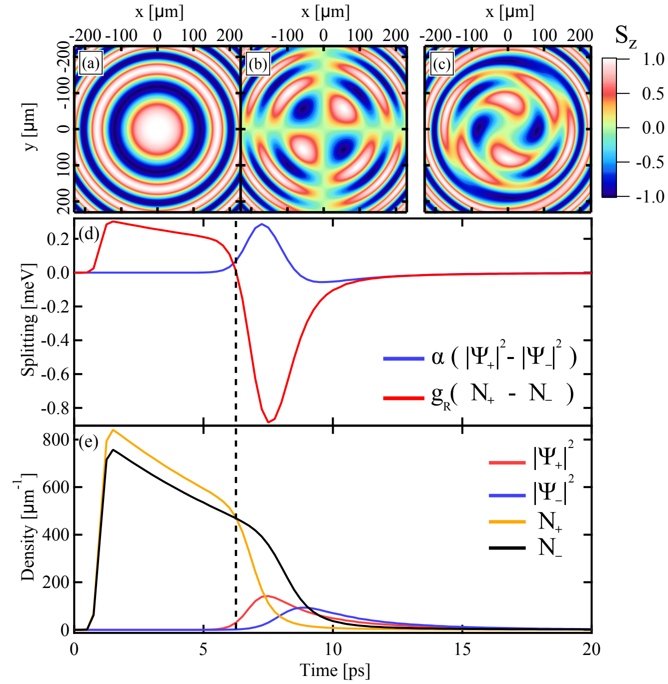

Figure 2. (a-c) Spin textures showing the evolution of the degree of circular polarization S_z after 50 ps in a system excited with (a) nearly circular ($\sigma_+ = 1; \sigma_- = 0.1$), (b) linear ($\sigma_+ = \sigma_- = 1$) and (c) elliptical ($\sigma_+ = 1; \sigma_- = 0.9$) pump polarization. (d-e) Dynamics of the condensate and reservoir at the pump position under elliptical pumping. (d) Energy splitting versus time of the polariton condensate (blue line) and exciton reservoir (red line). (e) Density versus time of the $\Psi_\pm$ polariton condensate and $\mathcal{N}_\pm$ exciton reservoir at the pump position. The dashed line indicates the position where the energy splitting in (d) reverse.

B. Spin whirls origin

To understand this behavior, we must first consider that polaritons can only be generated in the vicinity of the localized pump spot, which serves as the source for the entire spatial spin pattern. The time-dependent spatial rotation observed in our configuration is, in fact, a manifestation of varying polarization at the pump spot location.

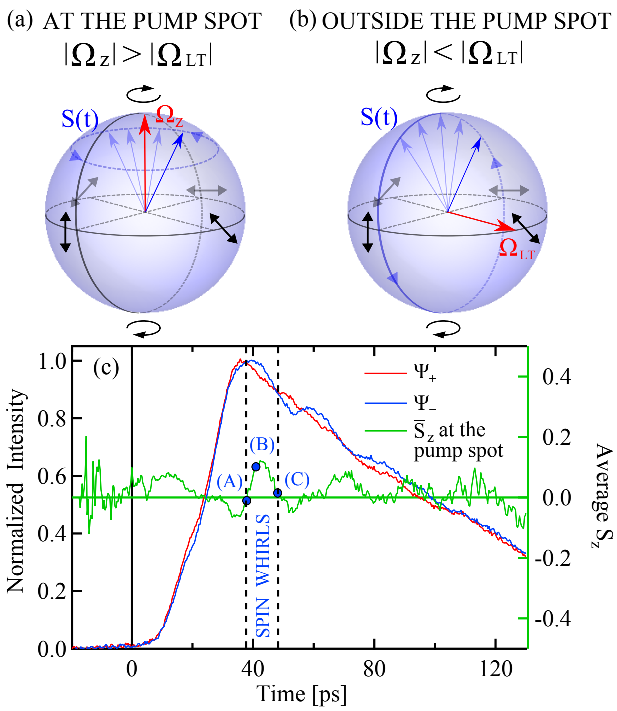

Figure 3. The pseudospin vector S(t) (blue arrows) in the Poincaré sphere at: (a) the pump spot and (b) outside the pump. At the pump spot position, (a), S(t) precesses around the z-direction since $|\Omega_z| > |\Omega_{LT}|$. Outside the pump spot, (b), S(t) precess around Ω_{LT} since $|\Omega_{LT}| > |\Omega_z|$.(c) Time-resolved, spatially integrated measurements of the two circular polarization components (Ψ_+, red and Ψ_-, blue) PL intensity, normalized and integrated over the area imaged in Figs. 1(a-c), i.e., $(460\,\text{x}\,340)\,\mu m^2$. In green we show the time resolved degree of circular polarization S_z averaged over an area $(1.78\text{x}1.78)\mu m^2$, centered at $(0,0)\mu m$ in Figs. 1(a-c), comparable with the 2 μm FWHM excitation spot. The blue solid circles annotated with (A), (B), (C) refer to the three snapshots of Figs. 1(a-c).

The varying polarization at the pump spot is generated by the ellipticity of the Gaussian pump, which populates one circular component of the reservoir faster than the other. This leads to a splitting $g_R(\mathcal{N}_+ - \mathcal{N}_-)$ of polaritons (Fig. 2(d)), which can be thought of as an effective Zeeman splitting at the pump spot. Here, the imbalance between the two populations [Fig. 2 (e)] induces an effective magnetic field along the z-direction (Ω_z) [39], which causes the precession of the Stokes vector in the Poincaré sphere, as shown schematically in Fig. 3 (a). Due to its excitonic nature, Ω_z exists only at the pump spot position where the exciton reservoir is localized. Away from the excitation spot, the polariton pseudospin dynamics is essentially driven by the TE-TM splitting of the polariton mode, represented by an in-plane effective magnetic field, Ω_{LT} [18] [Fig. 3(b)]. The combination of these two rotations is at the origin of the polariton spin whirls. The rotating polarization at the source results in the appearance of rotating spiral arms in the spatial distribution of the circular polarization degree, in analogy to the water jets created by a rotating sprinkler head [Figs. 1 (d-f)]. The energy splitting between Ψ_+ and Ψ_- states at the pump spot can also be generated by interactions between polaritons, $\alpha(|\Psi_+|^2 - |\Psi_-|^2)$, where the corresponding precession in linear polarization was previously described [40], however, we find that the dominant contribution to the splitting is caused by the exciton reservoir splitting, $g_R(\mathcal{N}_+ - \mathcal{N}_-)$ (see supplementary information [29], S4). The small imbalance between Ψ_+ and Ψ_-, induced by the ellipticity of the pump polarization, results in picosecond scale oscillation in the circular emission [red and blue profile in Fig. 3 (c)] indicated in the literature as features of bosonic stimulation[41,42]. Experimentally, the rotation of the polarization at the pump spot is confirmed by the average of the degree of circular polarization calculated at the pump spot position, which oscillates between ± 0.1, as shown in Fig. 3 (c) (green profile) and coincides with the rotation of the spin textures [Figs.1 (a-c)]. The differences in the time dynamics observed in experiment and theory are due to differences in the reservoir dynamics occurring at the pump spot position. Typically polariton condensation is described with the use of a single reservoir model [16]. While modeling using multiple reservoir levels may offer a closer fit to the dynamics [43,44], we do not expect significant changes in the spatial patterns, which are the main focus of our work.

C. Additional measurements

We have repeated the same experiments at the same conditions of detuning, power and excitation spot-size but now exciting with a circularly polarized beam (see supplementary information [29], S5 and video S3). In this case, polariton condensation results in highly imbalanced population [Fig. S4 (b)] and the small ellipticity induced by the tightly focused spot will not play a relevant role as in the case of linearly polarized pump. As a consequence, the imbalance between the two polariton populations is set by the pump and preserved throughout the entire process so that no oscillation of the polarization appear at the pump spot [Fig. S6 (d)] and the spin texture does not rotate (see supplementary information [29], S5).

Finally, we study the rotation of the spin textures using real-space spectral tomography under the same excitation conditions as in Fig. 1 (a-c). This is shown in Fig. 4. Under non-resonant optical excitation, the pseudospin

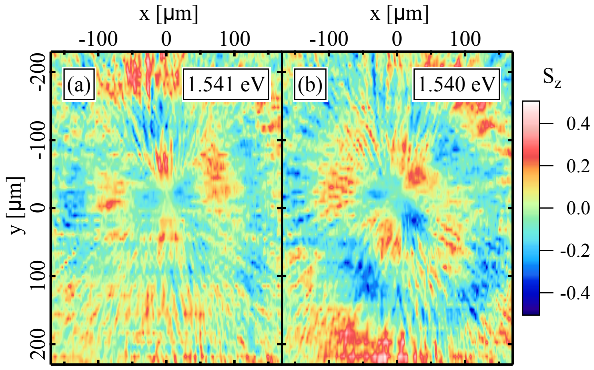

Figure 4. Snapshots of real space, spectral tomography of the degree of circular polarization S_z at: (a) 1.541 eV and (b) 1.540 eV showing the clockwise rotation of the spin whirls within the microcavity plane under non-resonant linearly polarized excitation.

dynamics of polaritons is strongly connected with the energy relaxation of the exciton reservoir immediately after the arrival of the excitation pulse. The decay of the exciton reservoir in time results to a gradual decreasing potential energy that polaritons experience at the pump spot. The interplay between the polariton spin and the energy relaxation of the exciton reservoir give rise to spin textures with different chirality (i.e., their image does not coincide with their respective mirror image) at different energies, similarly to the spin vortices at different energy observed in atomic condensate with ferromagnetic interactions [4]. The typical quadrature of the OSHE rotates by $\sim 45°$ in the plane of the microcavity due to the rotation of the linear polarization axis by $\sim 90°$ in the Poincaré sphere. This is also confirmed in k-space (see supplementary information [29], video S4), where the variation of the linear polarization at the source results in the appearance of rings of opposite circular polarization [45]. Thus, due to the varying polarization at the pump spot and the decrease of the blue shift with time, polaritons with spin up/down populate concentric rings in k-space (see supplementary information [29], video S4).

VI. CONCLUSIONS

In conclusion, we have observed and studied the dynamics of spin whirls in polariton microcavities. We demonstrated that the appearance of spin whirls is due to a dynamical optical spin Hall effect, which originates from the TE-TM splitting of propagating modes and a self-induced Zeeman splitting at the pump spot. The strong nonlinear interactions between polaritons and the exciton reservoir induce a collective rotation of the 2D textures in the plane of the microcavity. An analogous but static pattern of indirect exciton spin currents was observed under continuous wave excitation and a real magnetic field in coupled quantum wells [46]. Here, we emphasize the dynamic induction of an effective magnetic field on the picosecond scale and the resulting dynamic control of spin currents, which is an additional step toward the realization of spinoptronic devices.

ACKNOWLEDGMENTS

P.C. and P.G.L. acknowledge P.G. Savvidis and Z. Hatzopoulos for providing the sample. P.C. and P.G.L. acknowledge support by the Engineering and Physical Sciences Research Council, UK [Project EP/M025330/1]. H.S. and I.S. acknowledge support by the FP7 IRSES POLATER, ITN NOTEDEV and Rannis “Bose, Fermi and hybrid systems for spintronics”.

[1] D. A. Butts and D. S. Rokhsar, Nature **397**, 327 (1999).
[2] R. M. Wilson, B. M. Anderson, and C. W. Clark, Phys. Rev. Lett. **111**, 185303 (2013).
[3] L. S. Leslie, A. Hansen, K. C. Wright, B. M. Deutsch, and N. P. Bigelow, Phys. Rev. Lett. **103**, 250401 (2009).
[4] H. Saito, Y. Kawaguchi, and M. Ueda, Phys. Rev. Lett. **96**, 065302 (2006).
[5] Y. Dong, L. Dong, M. Gong, and H. Pu, Nat Commun **6** (2015), 10.1038/ncomms7103.
[6] D. Hsieh, Y. Xia, L. Wray, D. Qian, A. Pal, J. H. Dil, J. Osterwalder, F. Meier, G. Bihlmayer, C. L. Kane, Y. S. Hor, R. J. Cava, and M. Z. Hasan, Science **323**, 919 (2009).
[7] X. Z. Yu, Y. Onose, N. Kanazawa, J. H. Park, J. H. Han, Y. Matsui, N. Nagaosa, and Y. Tokura, Nature **465**, 901 (2010).
[8] M. I. Dyakonov and V. I. Perel, Physics Letters A **35**, 459 (1971).
[9] Y. K. Kato, R. C. Myers, A. C. Gossard, and D. D. Awschalom, Science **306**, 1910 (2004).
[10] L. E. Sadler, J. M. Higbie, S. R. Leslie, M. Vengalattore, and D. M. Stamper-Kurn, Nature **443**, 312 (2006).
[11] K. Shibata, X. Z. Yu, T. Hara, D. Morikawa, N. Kanazawa, K. Kimoto, S. Ishiwata, Y. Matsui, and Y. Tokura, Nat Nano **8**, 723 (2013).
[12] A. Fert, V. Cros, and J. Sampaio, Nat Nano **8**, 152 (2013).
[13] A. Kavokin, J. J. Baumberg, G. Malpuech, and F. P. Laussy, *Microcavities* (OUP Oxford, 2007).
[14] T. Byrnes, N. Y. Kim, and Y. Yamamoto, Nat Phys **10**, 803 (2014).
[15] J. Kasprzak, M. Richard, S. Kundermann, A. Baas, P. Jeambrun, J. M. J. Keeling, F. M. Marchetti, M. H. Szymanska, R. Andre, J. L. Staehli, V. Savona, P. B. Littlewood, B. Deveaud, and L. S. Dang, Nature **443**, 409 (2006).
[16] M. Wouters, I. Carusotto, and C. Ciuti, Phys. Rev. B **77**, 115340 (2008).
[17] A. Kavokin, P. G. Lagoudakis, G. Malpuech, and J. J. Baumberg, Phys. Rev. B **67**, 195321 (2003).

[18] A. Kavokin, G. Malpuech, and M. Glazov, Phys. Rev. Lett. **95**, 136601 (2005).
[19] C. Leyder, M. Romanelli, J. P. Karr, E. Giacobino, T. C. H. Liew, M. M. Glazov, A. V. Kavokin, G. Malpuech, and A. Bramati, Nature Physics **3**, 628 (2007).
[20] M. Maragkou, C. E. Richards, T. Ostatnický, A. J. D. Grundy, J. Zajac, M. Hugues, W. Langbein, and P. G. Lagoudakis, Opt. Lett. **36**, 1095 (2011).
[21] G. Panzarini, L. C. Andreani, A. Armitage, D. Baxter, M. S. Skolnick, V. N. Astratov, J. S. Roberts, A. V. Kavokin, M. R. Vladimirova, and M. A. Kaliteevski, Phys. Rev. B **59**, 5082 (1999).
[22] W. Langbein, I. Shelykh, D. Solnyshkov, G. Malpuech, Y. Rubo, and A. Kavokin, Phys. Rev. B **75**, 075323 (2007).
[23] E. Kammann, T. C. H. Liew, H. Ohadi, P. Cilibrizzi, P. Tsotsis, Z. Hatzopoulos, P. G. Savvidis, A. V. Kavokin, and P. G. Lagoudakis, Phys. Rev. Lett. **109**, 036404 (2012).
[24] M. Steger, G. Liu, B. Nelsen, C. Gautham, D. W. Snoke, R. Balili, L. Pfeiffer, and K. West, Phys. Rev. B **88**, 235314 (2013).
[25] P. G. Lagoudakis, P. G. Savvidis, J. J. Baumberg, D. M. Whittaker, P. R. Eastham, M. S. Skolnick, and J. S. Roberts, Phys. Rev. B **65**, 161310 (2002).
[26] T. C. H. Liew, I. A. Shelykh, and G. Malpuech, Physica E: Low-dimensional Systems and Nanostructures **43**, 1543 (2011).
[27] M. De Giorgi, D. Ballarini, P. Cazzato, G. Deligeorgis, S. I. Tsintzos, Z. Hatzopoulos, P. G. Savvidis, G. Gigli, F. P. Laussy, and D. Sanvitto, Phys. Rev. Lett. **112**, 113602 (2014).
[28] T. Gao, C. Antón, T. C. H. Liew, M. D. Martín, Z. Hatzopoulos, L. Viña, P. S. Eldridge, and P. G. Savvidis, Applied Physics Letters **107**, 011106 (2015).
[29] *See Supplemental Material*.
[30] M. Wouters and I. Carusotto, Phys. Rev. Lett. **99**, 140402 (2007).
[31] C. Ciuti, V. Savona, C. Piermarocchi, A. Quattropani, and P. Schwendimann, Phys. Rev. B **58**, 7926 (1998).
[32] M. Vladimirova, S. Cronenberger, D. Scalbert, K. V. Kavokin, A. Miard, A. Lemaitre, J. Bloch, D. Solnyshkov, G. Malpuech, and A. V. Kavokin, Phys. Rev. B **82**, 075301 (2010).
[33] N. Takemura, S. Trebaol, M. Wouters, M. T. Portella-Oberli, and B. Deveaud, Phys. Rev. B **90**, 195307 (2014).
[34] *In all the theoretical calculations the following parameters were set to:* $\alpha = 2.4\ \mu eV\ \mu m^2$, $g_R = 1.5\alpha$, $G = 4\alpha$, $r_c = 0.01\ \mu m^2\ ps^{-1}$, $\Delta_{LT}/k_{LT}^2 = 11.9\ \mu eV\ \mu m^2$, $\tau_p = 9$ *ps*, $\tau_x = 10$ *ps*.
[35] M. Combescot, O. Betbeder-Matibet, and R. Combescot, Phys. Rev. Lett. **99**, 176403 (2007).
[36] H. Flayac, D. D. Solnyshkov, I. A. Shelykh, and G. Malpuech, Phys. Rev. Lett. **110**, 016404 (2013).
[37] B. Richards and E. Wolf, Proceedings of the Royal Society of London A: Mathematical, Physical and Engineering Sciences **253**, 358 (1959).
[38] Z. Chen, L. Hua, and J. Pu, in *Progress in Optics*, Progress in Optics, Vol. 57, edited by E. Wolf (Elsevier, 2012) pp. 219–260.
[39] P. Renucci, T. Amand, X. Marie, P. Senellart, J. Bloch, B. Sermage, and K. V. Kavokin, Phys. Rev. B **72**, 075317 (2005).
[40] I. Shelykh, K. V. Kavokin, A. V. Kavokin, G. Malpuech, P. Bigenwald, H. Deng, G. Weihs, and Y. Yamamoto, Phys. Rev. B **70**, 035320 (2004).
[41] M. D. Martin, G. Aichmayr, L. Viña, and R. André, Phys. Rev. Lett. **89**, 077402 (2002).
[42] I. A. Shelykh, A. V. Kavokin, and G. Malpuech, phys. stat. sol. (b) **242**, 2271 (2005).
[43] K. G. Lagoudakis, F. Manni, B. Pietka, M. Wouters, T. C. H. Liew, V. Savona, A. V. Kavokin, R. André, and B. Deveaud-Plédran, Phys. Rev. Lett. **106**, 115301 (2011).
[44] C. Anton, T. C. H. Liew, G. Tosi, M. D. Martin, T. Gao, Z. Hatzopoulos, P. S. Eldridge, P. G. Savvidis, and L. Vina, Phys. Rev. B **88**, 035313 (2013).
[45] A. Amo, T. C. H. Liew, C. Adrados, E. Giacobino, A. V. Kavokin, and A. Bramati, Phys. Rev. B **80**, 165325 (2009).
[46] A. A. High, A. T. Hammack, J. R. Leonard, S. Yang, L. V. Butov, T. Ostatnický, M. Vladimirova, A. V. Kavokin, T. C. H. Liew, K. L. Campman, and A. C. Gossard, Phys. Rev. Lett. **110**, 246403 (2013).